J Ind Microbiol Biotechnol (2015) 42:723–734
DOI 10.1007/s10295-015-1602-0

BIOTECHNOLOGY METHODS

SIMB
Society for Industrial Microbiology and Biotechnology

Mussel-inspired surface modification of magnetic@graphite nanosheets composite for efficient Candida rugosa lipase immobilization

Chen Hou · Lincheng Zhou · Hao Zhu · Xinyu Wang · Niran Hu · Fang Zeng · Liyuan Wang · Hang Yin

Received: 7 September 2014 / Accepted: 29 January 2015 / Published online: 10 March 2015

Abstract By the facile adhesion way, the novel composite complex by polydopamine (PDA) and magnetic graphite nanosheets (Fe_3O_4@GNSs) has been successfully synthesized. The resulting composite was characterized by means of scanning electron microscopy, transmission electron microscopy, Fourier transform infrared spectra, and Raman spectra, X-ray diffraction, X-ray photoelectron spectroscopy, and vibrating sample magnetometry. Meanwhile, the PDA functionalized Fe_3O_4@GNSs (Fe_3O_4@GNSs-PDA) was applied for Candida rugosa lipase (CRL) immobilization covalently without any toxic coupling agent. Combining the superior physical properties and chemical stability of Fe_3O_4@GNSs and the well biocompatibility, functional characteristics of PDA, the Fe_3O_4@GNSs-PDA composite displayed several advantages, including the high enzyme capacity, enzyme activity and stability and a decrease in enzyme loss. Our work demonstrated that the mussel-inspired Fe_3O_4@GNSs can be extended to many other applications such as biocatalytic, genetic and industrial.

Chen Hou and Hao Zhu contributed equally to this work.

This paper is dedicated to memory of pro. Yanfeng Li, who passed away recently.

Electronic supplementary material The online version of this article (doi:10.1007/s10295-015-1602-0) contains supplementary material, which is available to authorized users.

C. Hou · L. Zhou · H. Zhu (✉) · X. Wang · N. Hu · F. Zeng · L. Wang · H. Yin
State Key Laboratory of Applied Organic Chemistry, Key Laboratory of Nonferrous Metal Chemistry and Resources Utilization of Gansu Province, College of Chemistry and Chemical Engineering, Institute of Biochemical Engineering and Environmental Technology, Lanzhou University, Lanzhou 730000, China
e-mail: zhuhao07@lzu.edu.cn

Keywords Magnetic composite · Polydopamine · Enzyme immobilization · Enzyme activity · Thermostability

Introduction

Immobilization of biocatalysts has been generally adapted for synthesis of high stereoselectivity and enantioselectivity products with the consideration of green, economic and sustainable chemistry. Enzymes are an important group of biocatalysts superior to chemical catalysts because of their high effectiveness, high specificity, and green reaction conditions [1]. Enzymes have found practical use in industrial processes and are extensively used in new fields, such as bioengineering [2], food industry [3], pharmaceuticals [4], fine chemical industry, biosensors, and biofuel cells [5]. However, the poor catalytic activity, stability and selectivity as well as recycling problems of free enzymes limited the applications in extensive fields [6]. In order to increase the performance of enzymes, many supporting materials have been developed including polysaccharide [7], inorganic materials [8, 9], organic polymeric carriers [10], and natural polymers [11], etc. Nevertheless, aiming at design facile, universal, economical, and environmental friendly supporting materials in balancing the key factors, which determine the efficiency of biocatalysts, including surface area, mass transfer resistance, and effective enzyme loading still remains challenging.

Graphite, with the excellent mechanical, thermal, optical, and electrical properties [12], simulated ever-increasing attention, and various kinds of graphite series based matrix and hybrids have been prepared for compound and immobilization [13–15]. Combining the merits of the unique magnetic properties of Fe_3O_4 nanoparticles and

chemical stability, non-toxicity of graphite nanosheets, the magnetic nanoparticles doped graphene or graphite composites have been caused excited interests and used as carriers of drug delivery, purification and detection of biomolecules, immobilization of enzymes, and enrichment of proteins recently [16–19]. Chen and co-workers fabricated electrically and magnetically bi-functional graphene/γ-Fe_2O_3 hybrid aerogels for immobilizing β-glucuronidase [20]. Ma et al. [21] developed a cost-effective way to prepare Fe_3O_4 and graphite nanosheets composite to immobilize glucoamylase covalently by an inverse co-precipitation method. Taking advantage of the high loading capacity and abundant hydrophilic groups of graphene oxide (GO), and large surface areas and hydrophobicity of reduced graphene oxide (rGO), Chen et al. [22] prepared strong magnetic GO-Fe_3O_4 and rGO-Fe_3O_4 for the immobilization of protein and the enrichment of peptides, respectively. Li et al. [23] introduced an easy one-pot polyol approach to hybridize size- and density-tunable graphene-Fe_3O_4 composites for the immobilization of porcine pancreatic lipase. Despite these developments, there is still a need for some chemical modification schemes of magnetic graphene or graphite nanosheets that can derivatize a variety of materials in bio-applications.

Dopamine (DA) mimics the repetitive catechol-amine structure of 3,4-dihydroxyl-L-phenylalanine found in mussel's foot protein, which has excellent adhesion property with virtually all organic and inorganic surfaces [24]. Polydopamine (PDA) has recently been introduced by Lee et al. who reported its versatility for various substrates and feasibility for facile functionalization with spontaneous oxidative polymerization of DA under mild conditions [25]. Since then, dopamine was utilized as a versatile and intriguing starting material for almost all kinds of solid surface modifications very extensively due to the green, simple, fast, and low-cost synthesis approach [26–28]. Especially, the coated polydopamine films also can be used for the step-functionalization with organic species for the creation of functional organic ad-layers [29, 30].

Although the utilization of magnetic graphite nanosheets and DA for immobilization has been reported several times, the composite that combines the excellent properties of both of them by facile adhesion way is still very innovative. Herein, inspired by the adhesion mechanism of mussels, we utilized DA as an attractive functional monomer for the modification of Fe_3O_4 decorated graphite nanosheets (Fe_3O_4@GNSs) for enzyme immobilization.

In this work, we prepared the non-toxic, high affinity and rapid magnetic response magnetic graphite nanosheets composite via a one-pot hydrothermal approach, and the polydopamine-coated Fe_3O_4@GNSs composite was then fabricated by in situ polymerization of dopamine. Then enzymes could be immobilized on polydopamine-coated Fe_3O_4@GNSs composite via Schiff base reaction. The Candida rugosa lipase (CRL) was used as the target enzyme because of the specific property and the increased activity when bound to an interface [31]. Thanks to the combination of high capacity, superior physical stability of GNSs and well biocompatibility, functional characteristics of PDA, the Fe_3O_4@GNSs-PDA composite shows the high performance as an enzyme immobilization supporting material. Moreover, the enzyme immobilized on Fe_3O_4@GNSs-PDA composite would promise to be a novel nano-biosensor and nano-reactor for the catalytic reaction.

Materials and methods

Materials

Natural flake graphite (NFG) 50 BS mesh, with the purity of 99 wt % was used as a precursor for the synthesis of GNSs supplied by ShanDong Qingdao Tianhe Graphite Company (China). Dopamine hydrochloride (DA), ethylene glycol (EG), sodium acetate (NaAc) and $FeCl_3{\cdot}6H_2O$ were purchased from AiHua Fine Chemicals Co., Ltd. (China). Candida rugosa lipase (CRL, Type VII) and bovine serum albumin (BSA) were purchased from Sigma Chemical Co. Other chemicals and reagents were of analytical grade, obtained from Tianjing Chemical Reagent Company (China).

Characterization

Fourier transform infrared (FTIR) spectra were obtained in transmission mode on a FT-IR spectrometer (American Nicolet Corp., Model 170-SX) using the KBr pellet technique. Raman spectra were carried out via a Reinishaw confocal spectrometer with 633 nm laser. Powder X-ray diffraction (XRD, Rigaku D/MAX-2400 X-ray diffractometer with Ni-filtered Cu Kα radiation ($\lambda = 1.54056$)) was used to investigate the crystal structure of the composites. All spectra were recorded under the same experimental conditions. The morphologies of the Fe_3O_4@GNSs and Fe_3O_4@GNSs-PDA were characterized by a field-emission scanning electron microscope (SEM, Hitachi S-4800, Japan), transmission electron microscope (TEM, FEI Tecnal G^2F30) equipped with energy-dispersive X-ray spectroscopy (EDX, Oxford Instrument), high angle annular dark field (HAADF) and scanning transmission electron microscopy (STEM) to elucidate the dimensions and the structural details of the composites. The surface composition and oxidation state of the samples were performed by X-ray photoelectron spectroscopy (XPS, ESCALAB210). Magnetization measurements were characterized on a vibrating sample magnetometer (Lakeshore 7304, USA) at room temperature. The thermal stability

of samples was studied with a thermogravimetry (TG) analyzer (STA449C, Netzsch, Germany) at heating rate of 10 °C min^{-1} in a nitrogen atmosphere.

Preparation of GNSs

GNSs were prepared according to the previous work of our group [21]. Typically, the mixed acidic intercalating agent was collocated with 70 % concentrated sulfuric acid (45 g) and 68 % nitric acid (15 g). Then 20 g of NFG was added slowly to the mixed acid in a small portion, and 2.2 g $KMnO_4$ was dissolved into this mixture. The NFG was oxidized for 50 min under continuous stirring. Afterwards, the resulting solid mixture was washed with distilled water and a neutral elution solution through a centrifuge process was obtained; the precipitate was dried at 60 °C. The dried sample, i.e., graphite oxide (GO) was heat-treated abruptly at 600 °C for 15 s to obtain expanded GO. Then, dimethyl formamide (DMF) was used as dispersing agent to peel off the expanded GO. The prepared expanded GO was immersed in a dimethyl formamide (DMF) solution (2 mg/ml) in an ultrasonic bath and sonicated for 12 h, and lastly was filtered and dried to produce the graphite nanosheets (GNSs).

Preparation of Fe_3O_4@GNSs

An easy one-pot method was employed for preparation of Fe_3O_4@GNSs composite via a solvothermal method. In a typical procedure, GNSs (0.1 g) was added into ethylene glycol (30 ml) and ultrasounded under drastic stirring for 1 h. Then $FeCl_3{\cdot}6H_2O$ (0.487 g) and sodium acetate (NaAc, 0.973 g) were dispersed into the aforementioned solution under continuous stirring so that Fe^{3+} chemically bonded onto expanded GO. After complete dissolution, the rich dark brown solution was transferred into a 50 mL Teflon reactor and heated at 200 °C for 8 h. After cooling down to room temperature (~20 °C), the solid product was gained by magnetic separation, and washed with deionized water and ethanol repeatedly several times. Finally the product was dried in vacuum at 40 °C for 8 h to obtain the uniform Fe_3O_4 nanoparticles embedded in GNSs.

Preparation of polydopamine modified Fe_3O_4@GNSs

The surface modification of Fe_3O_4@GNSs can be easily manipulated using dopamine with spontaneous oxidative polymerization under mild conditions. In a typical procedure, Fe_3O_4@GNSs (50 mg) was sonicated in a buffered solution (10 Mm Tris–HCl buffer, pH 8.5) for 30 min, and then a corresponding amount of dopamine (2 mg/ml) was added into the above suspension under vigorous stirring for a desired reaction time. The PDA-coated Fe_3O_4@GNSs was thoroughly rinsed with deionized water and ethanol repeatedly and then dried in a vacuum at room temperature for 8 h.

Immobilization of CRL

The CRL was immobilized onto Fe_3O_4@GNSs-PDA composite mainly via covalent binding [32]. Necessary quality of support was put into CRL solution (m/v, 1 %); then the lipase immobilization was carried out at 30 °C in a shaking-table with rotational speed at 120 rpm min^{-1} for 5 h. After the reaction was completed, the immobilized CRL was obtained by magnetic separation and washed with phosphate buffer (0.1 M, pH = 7.0) several times to remove the unreacted CRL. Especially, the reaction solution and washing solution were collected to assay the amount of residual lipase. The ICRL was kept at 4 °C prior to use.

During the immobilization procedure, the amount of lipase added and reaction time on the activity of immobilized lipase were investigated. The relative activity was obtained after incubation under different amount of lipase added (100–500 mg/g support), immobilizing time (1–9 h), respectively.

Determination of immobilization efficiency and lipase activity

The immobilization efficiency was expressed by the amounts of enzyme bounded on supports of unite mass, and using BSA as the standard to determine the amount of enzyme by the Bradford method [33]. The enzymatic activities of free and immobilized lipase were measured by the titration of the fatty acid which comes from the hydrolysis of olive oil [34] and reverse titration was adopted. One unit of lipase activity (U) is defined as the amount of enzyme needed to hydrolyze olive oil liberating 1.0 μmol of fatty acid per min in the assay condition.

The efficiency of immobilization was evaluated in terms of activity yields and immobilization yield as follows:

$$\text{activity yield (\%)} = \frac{C}{A}100\,\%$$

$$\text{immobilization yield (\%)} = \frac{A-B}{A}100\,\%$$

where A is the activity of lipase added in the initial immobilization solution, B is the total activity of the residual lipase in the immobilization and washing solution after the immobilization procedure, and C is the activity of the immobilized lipase, respectively.

The relative activity (%) is the ratio between the activity of each sample and the maximum activity of the sample.

The residual activity (%) is the ratio between the activity of each sample and the initial activity of the sample.

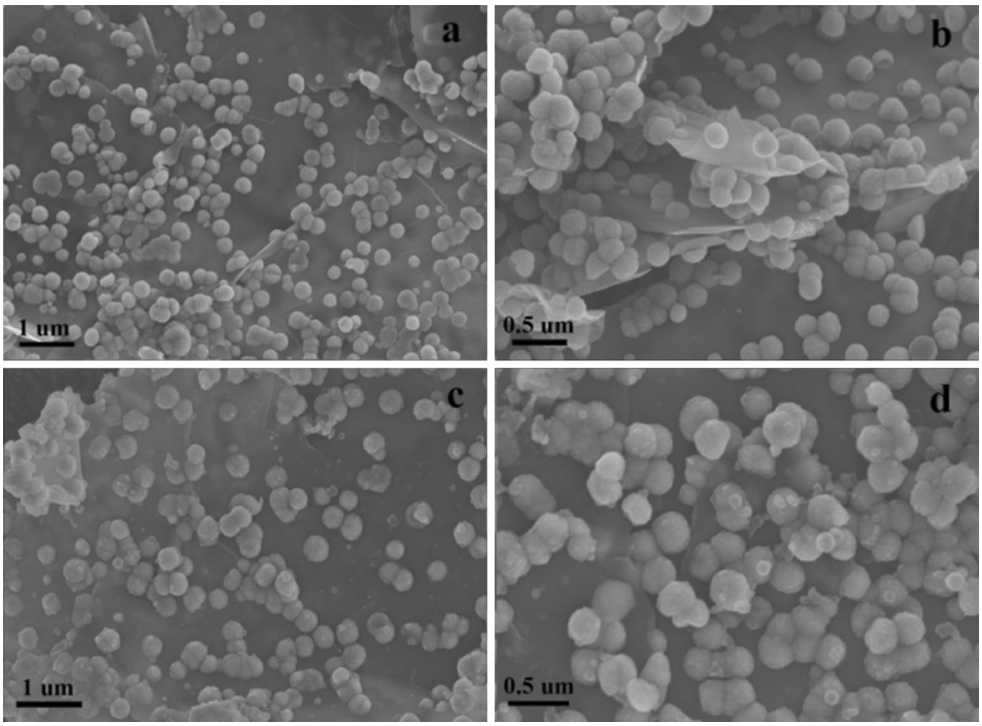

Fig. 1 SEM images of Fe_3O_4@GNSs (**a** and **b**) and Fe_3O_4@GNSs-PDA(**c** and **d**)

All data used in these formulas are the average of triplicate of experiments.

Properties of Fe_3O_4@GNSs-PDA immobilized CRL

Effect of pH and temperature of free and immobilized lipase activities

A certain amount of free and immobilized CRL was incubated in 0.1 M 50 ml phosphate buffer under various pH (3.0–10.0) at 37 °C for 30 min with continuous stirring, respectively. Then the enzymatic activities were determined and the relative activities were calculated.

The effect of temperature on the activities of free and immobilized CRL was investigated in the temperature range 20–90 °C for 30 min. The relative activities were calculated.

Thermal stability of free and immobilized lipase activities

Thermal stabilities of the free CRL and immobilized CRL were determined by measuring the activities following incubation in 50 ml phosphate buffer (0.1 M, pH = 7.0) at 50 °C for 240 min with continuous stirring. A sample was removed at 30 min interval and assayed for enzymatic activity. Residual activity was calculated as mentioned above.

Effect of denaturant of free and immobilized lipase activities

A series of concentrations of urea-phosphate buffer solution (0.1 M, pH = 7.0) were added into the hydrolysis reaction of olive oil using free and immobilized lipase at 30 °C, respectively. Then the residual activity of free lipase and of the ICRL was calculated.

Reusability of ICRL

The reusability of the immobilized CRL was determined by hydrolysis of olive oil by the recovered lipase after magnetic separation and compared with that of the first running (activity defined as 100 %).

Results

Preparation and characterization of Fe_3O_4@GNSs-PDA

The size and morphologies of Fe_3O_4@GNSs and Fe_3O_4@GNSs-PDA composites were characterized by SEM and TEM observations. Figure 1 shows SEM images of Fe_3O_4@GNSs and Fe_3O_4@GNSs-PDA composites. As can be seen from Fig. 1a, b, spherical Fe_3O_4 nanoparticles with a diameter about 300–350 nm deposited on the surface

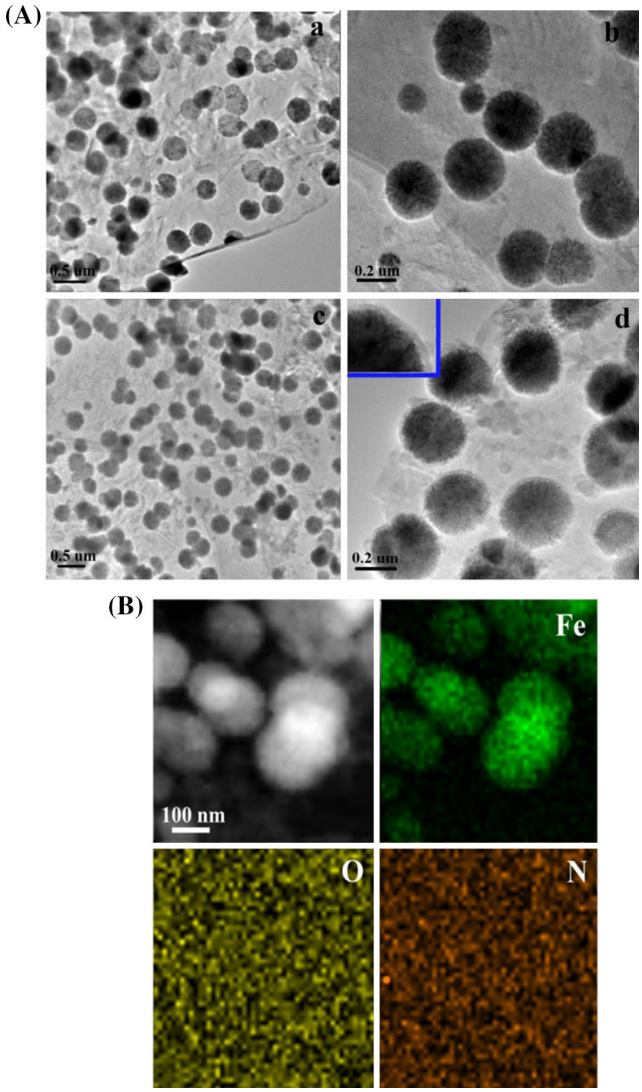

Fig. 2 **A** TEM images of Fe_3O_4@GNSs (*a* and *b*), and Fe_3O_4@GNSs-PDA (*c* and *d*), **B** STEM image and corresponding iron, oxygen, and nitrogen elemental mapping of Fe_3O_4@GNSs-PDA composite

or in the interlayer of GNSs uniformly, which owns to the controllable one-pot hydrothermal process. After the in situ polymerization reaction, PDA film was coated on Fe_3O_4@GNSs so that the surface of Fe_3O_4@GNSs became coarse (Fig. 1c, d) and the diameter of Fe_3O_4@GNSs-PDA composite increased by ~30 nm (Fig. 1d). TEM images present a consistent result compared with the SEM images. It is seen from Fig. 2A a, b, that Fe_3O_4 nanoparticles are an assembly of many small Fe_3O_4 nanocrystals [38] and well dispersed on GNSs, plenty of wrinkles of GNSs can be observed obviously due to the thin structure of the sheet. After the formation of Fe_3O_4@GNSs-PDA composite, a distinct gray thin PDA layer was wrapped on the Fe_3O_4 core (dark) and the surface of GNSs (gray) made it rough and thicker (Fig. 2A c, d). Energy-dispersive X-ray spectroscopy elemental mapping was used to understand the distribution of elements in the composites. From the elemental distribution of iron, oxygen and nitrogen in Fig. 2B, we can recognize that Fe, O and N are distributed uniformly throughout the specific area in Fe_3O_4@GNSs-PDA. Thus, we can speculate that the Fe_3O_4@GNSs was synthesized by the one-pot hydrothermal method and the PDA coating layer was successfully wrapped on the surface of Fe_3O_4@GNSs so that the enzyme would be immobilized on it.

FT-IR was employed to examine the surface composition of the synthesized GNSs, Fe_3O_4@GNSs and Fe_3O_4@GNSs-PDA composites. In the spectrum of bare GNSs (Fig. 3a), multiple peaks were observed in the range of 900 to 1,500 cm^{-1}, which can be assigned to the functional groups, including C–O (ν C–O at 1,060 cm^{-1}), C–O-C (ν C–O-C at 1,247 cm^{-1}), C = O in carboxylic acid and carbonyl moieties (ν C = O at 1,764 cm^{-1}). The intense band at 1,594 cm^{-1} attributed to the O–H bending vibration, epoxide groups and skeletal ring vibrations [39]. After decorated with Fe_3O_4, the strong peak at 579 cm^{-1} is related to the vibration of the Fe–O function group and peaks at 1,634 and 3,435 cm^{-1} are corresponding to the surface-adsorbed water and hydroxyl groups during the hydrothermal process. New peaks at 1,239, 1,293, 1,500 cm^{-1} and stronger peaks at 1,634 cm^{-1} in the spectrum of Fe_3O_4@GNSs-PDA derive from the aromatic rings in the PDA polymer. In addition, it could be noted that the peak at 3,435 cm^{-1} of Fe_3O_4@GNSs-PDA is broader than that of Fe_3O_4@GNSs, which resulted from the overlapping of hydroxyls, water adsorbed in PDA polymer and amines of PDA [40]. The FT-IR analysis suggested that PDA adhered onto Fe_3O_4@GNSs surface successfully.

In Raman spectrum (Fig. 3b), GNSs shows D-band peak at 1,332 cm^{-1} and G-band peak at 1,576 cm^{-1}, respectively [41]. The G-band is due to the first-order scattering of E_{2g} mode and is associated with the in-plane vibration of sp^2 carbon domains in a 2D hexagonal lattice, while the D-band arises from the κ-point phonons of A_{1g} mode and is related to the vibration of sp^3 carbon domains in plane terminations of disordered graphite [42]. Compared with pristine GNSs, the D- and G-bands of Fe_3O_4@GNSs become lower and broader, suggesting a higher level of disorder of the graphite layers during the functionalization process [43]. The G-bands of Fe_3O_4@GNSs, occur at 1,581 cm^{-1}, which is up shifted by 5 cm^{-1} compared to that of GNSs clearly demonstrates that there is a strong interaction between the Fe_3O_4 and GNSs. In the Raman spectra of Fe_3O_4@GNSs-PDA, the slightly split peak at 1,320 cm^{-1} with the sharp peak at 1,581 cm^{-1} can be characterized as the stretching and deformation of aromatic rings of PDA [44] which confirms the existence of PDA in Fe_3O_4@

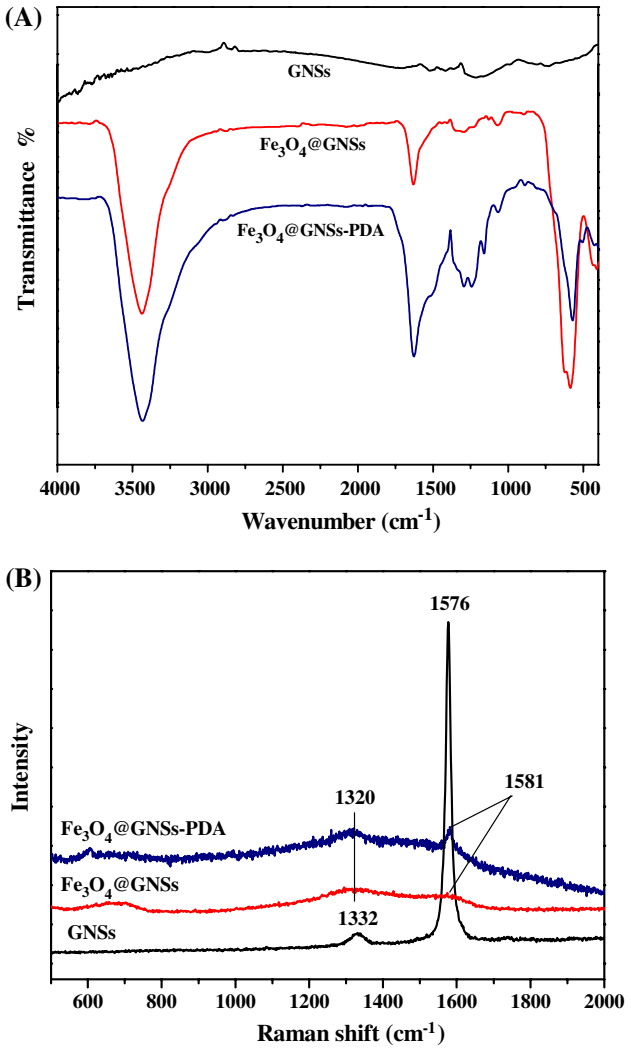

Fig. 3 **a** FT-IR spectra of GNSs, Fe_3O_4@GNSs and Fe_3O_4@GNSs-PDA, **b** Raman spectra of GNSs, Fe_3O_4@GNSs, and Fe_3O_4@GNSs-PDA

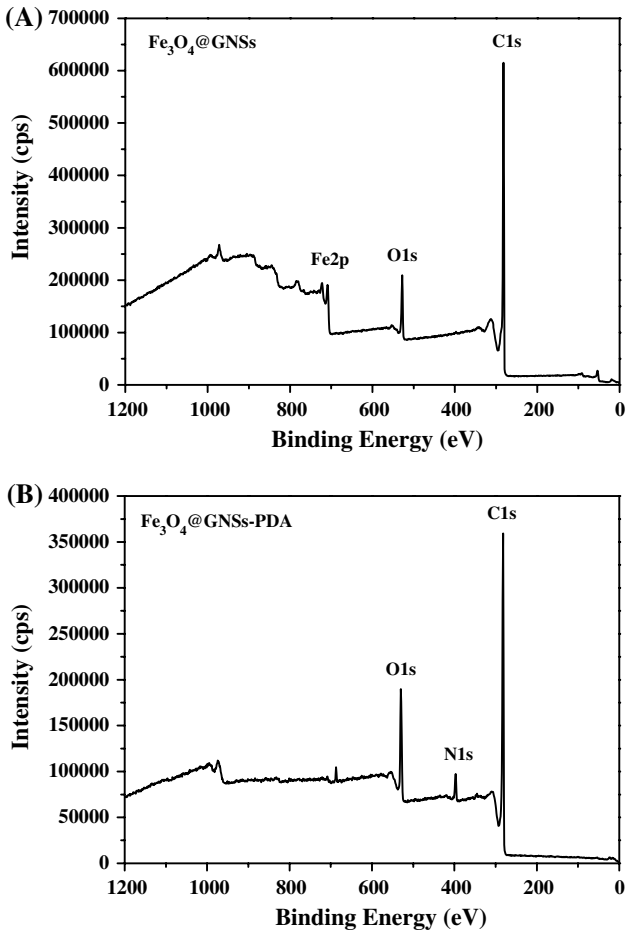

Fig. 4 **a** XPS spectra of Fe_3O_4@GNSs, **b** XPS spectra of Fe_3O_4@GNSs-PDA

GNSs-PDA composite. What is more, it can be seen from Fig. 3b that these two characteristic peaks became sharper and more obvious than that of Fe_3O_4@GNSs at the same position, which resulted from the overlap of the two peaks between PDA and the typical D- and G-bands of Fe_3O_4@GNSs. The similarity in FT-IR and Raman spectroscopy further supported the affinity between Fe_3O_4@GNSs and PDA film.

X-ray photoelectron spectroscopy (XPS) analysis was applied to investigate the chemical elements on surface of the materials. The wide-scan XPS spectra for Fe_3O_4 nanoparticles, Fe_3O_4@GNSs and Fe_3O_4@GNSs-PDA composites are shown in Fig. 4. As can be seen from Fig. 4a, except for the characteristic peaks of C1s and O1s, the spectrum of Fe2p appeared in the spectrum of Fe_3O_4@GNSs, and the high intensity C1s came from GNSs suggested the Fe_3O_4@GNSs was effectively obtained. After the Fe_3O_4@GNSs composite was wrapped by PDA film, the Fe_3O_4 peak from the underlying composite was screened (Fig. 4b), indicating that the surface was coated with a film that was thicker than the analysis depth of XPS (~10 nm). Meanwhile, a new peak of N1s in Fig. 4b appeared, and the nitrogen-to-carbon signal ratio (N/C) of 0.126 was similar to that of the theoretical value for PDA (N/C = 0.125), implying the formation of a polydopamine layer.

XRD was used to confirm the phase and structure of the prepared samples. Figure 5 shows that both Fe_3O_4@GNSs (Fig. 5a) and Fe_3O_4@GNSs-PDA (Fig. 5b) possess diffraction patterns similar to those of Fe_3O_4 (JCPDS no. 19–629): the 111, 220, 311, 400, 422, 511, 440 planes of Fe_3O_4 were observed at $2\theta = 18.25, 30.19, 35.39, 43.04, 53.44, 56.80, 62.46^{\circ}$, respectively. Meanwhile, the sharp diffraction peak at $2\theta = 26.50^{\circ}$ in Fe_3O_4@GNSs and Fe_3O_4@GNSs-PDA can be attributed to the graphite-like 002 reflection. This suggests that the crystal structure of the magnetite component was preserved during the whole synthesis process.

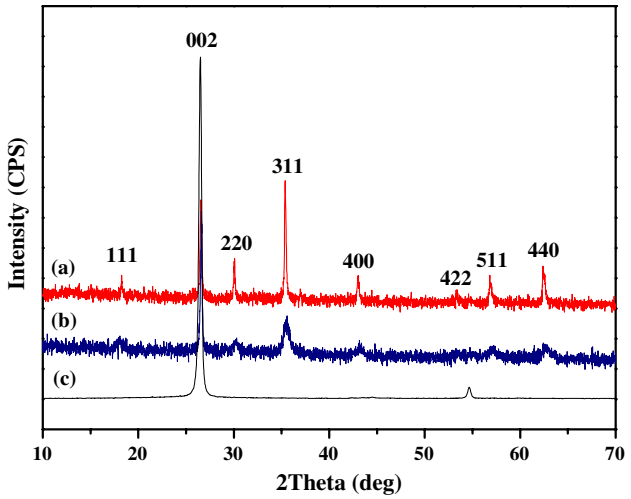

Fig. 5 XRD patterns of Fe_3O_4@GNSs (**a**), Fe_3O_4@GNSs-PDA (**b**), and GNSs (**c**)

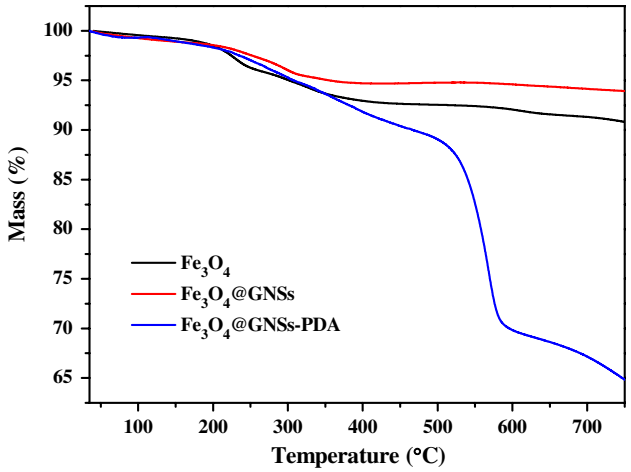

Fig. 6 TG curves of Fe_3O_4, Fe_3O_4@GNSs and Fe_3O_4@GNSs-PDA

For quantifying the amount of PDA in the Fe_3O_4@GNSs-PDA composite, thermogravimetric analysis (TGA) was carried out in nitrogen atmosphere at a rate of 10 °C min^{-1}. Figure 6 displayed the TGA curves of the Fe_3O_4@GNSs and Fe_3O_4@GNSs-PDA samples along with bare Fe_3O_4. As can be seen from Fig. 6, the Fe_3O_4@GNSs showed a mild weight loss (1.45 wt %) below 200 °C which can be assigned to the evaporation of absorbed water and solvent. The significant decomposition occurred between 200 and 400 °C (3.83 wt %) mainly due to the pyrolysis of stable oxygen-functioned groups. Compared with the Fe_3O_4@GNSs composite, bare Fe_3O_4 lost weight about 5.61 % at the temperature range 200–400 °C, which is indicative of the remarkable thermo-stability of Fe_3O_4@GNSs. The TG curve of Fe_3O_4@GNSs-PDA kept same trend between 35 and 400 °C, while a large mass loss (18.33 %) is observed from 513 to 589 °C which is presumed to result from the decomposition of PDA. The final weight loss of Fe_3O_4@GNSs-PDA is 35.10 %, indicating that PDA comprises about a half mass of the Fe_3O_4@GNSs-PDA.

In the use of PDA polymer coated Fe_3O_4@GNSs for lipase immobilization, it is important that the Fe_3O_4@GNSs-PDA should possess sufficient magnetic properties. The magnetic properties of bulk Fe_3O_4 nanoparticles, Fe_3O_4@GNSs and Fe_3O_4@GNSs-PDA composites were studied using a vibrating sample magnetometer at room temperature. From Fig. 7a we can see that the as-prepared magnetic materials have a fairly strong magnetization and the saturation magnetization (MS) values are about 84.57 emu g^{-1} for Fe_3O_4, 53.09 emu g^{-1} for Fe_3O_4@GNSs and 37.28 emu g^{-1} for Fe_3O_4@GNSs-PDA, respectively. The decrease in magnetic saturation of Fe_3O_4@GNSs-PDA in

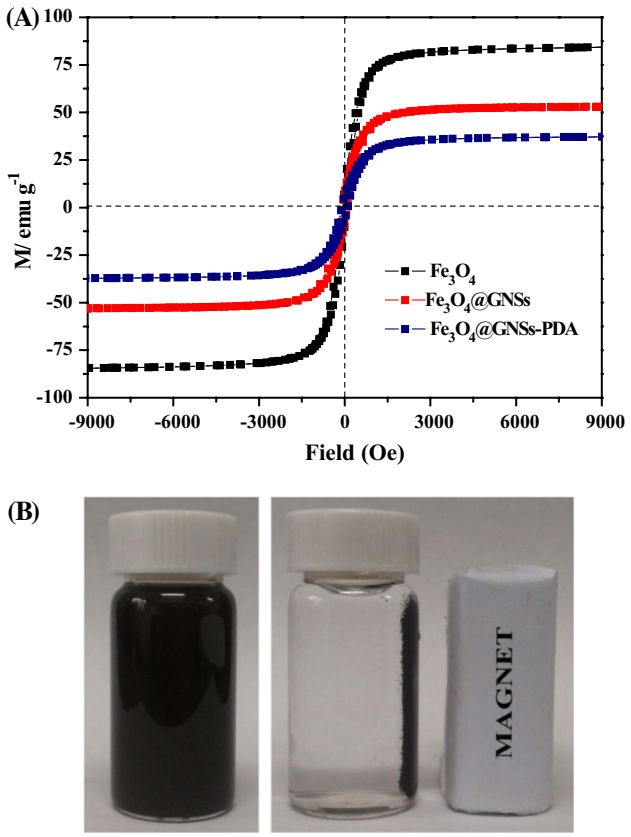

Fig. 7 **a** Magnetic hysteresis loops of Fe_3O_4, Fe_3O_4@GNSs and Fe_3O_4@GNSs-PDA, **b** Schematic of the simple magnetic separation of Fe_3O_4@GNSs-PDA

comparison with Fe_3O_4@GNSs may be attributed to the increased mass of modified polydopamine shell on the surface of Fe_3O_4@GNSs. The Fe_3O_4@GNSs-PDA composite also shows fast response to the applied magnetic field

(2000 Oe), and after dispersing the Fe_3O_4@GNSs-PDA in water by shaking, vortexing or sonication, it can be easily collected within several minutes by placing a magnet on the side of the vessel (Fig. 7b). Though the saturation magnetizations of Fe_3O_4@GNSs-PDA is lower than bulk Fe_3O_4 and Fe_3O_4@GNSs, it is strong enough for effective magnetic separation.

Activity of Fe_3O_4@GNSs-PDA immobilized CRL

Optimum conditions of ICRL

For the preparation of Fe_3O_4@GNSs-PDA immobilized CRL, the activity of lipase amount added is shown in Fig. 8a. From Fig. 8a we can see, with the lipase amount increased the activity of ICRL rose gradually and decreased after the lipase amount added was up to 350 mg g^{-1}. The excellent ability of lipase loading was much higher than our previous works [23, 47] which correlated to the high capacity of GNSs and high activity of PDA polymer both for chemistry and physics. The relative activity declined when the lipase amount added was up to 400 mg g^{-1} because of the over cross-linking of CRL during the immobilizing process. Relevant research confirmed that the improved activity of the immobilized lipase was involved with the alteration of its secondary structure, especially to the increase of α-helix content and the decrease of β-sheet content [48], which demonstrates that the Fe_3O_4@GNSs-PDA have well biocompatibility and affinity with CRL to enhance its activity.

Figure 8b shows the result of the immobilizing time of CRL. It can be seen that the optimum immobilizing time is 5 h, after 6 h the relative activity of ICRL decreased sharply. The main reason is that an appropriate reaction time contributed to couple the lipase on Fe_3O_4@GNSs-PDA, while the excessive coupling time may lead to the inactivation of CRL.

As a result, the optimum conditions of immobilizing lipase were obtained: amount of lipase was 350 mg g^{-1} support, reaction time was 5 h at pH value of the reaction system was 7.0. The bounded protein of the immobilized lipase under this condition was 337.96 mg g^{-1} support and the activity yield of the ICRL was 65.43 % (Table 1). Therefore, the results obtained in our work seemed to be quite promising.

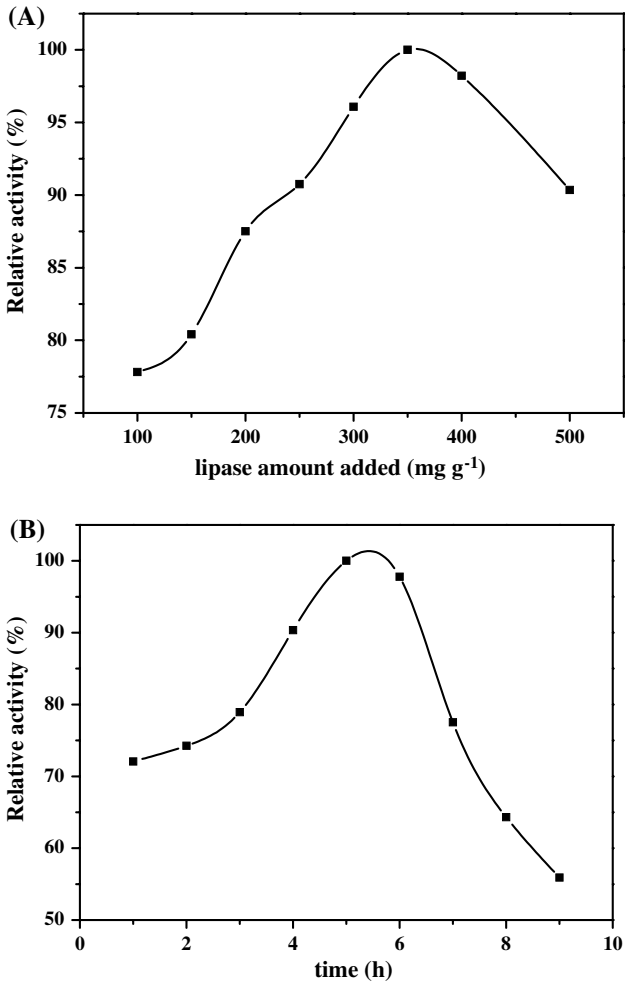

Fig. 8 **a** The effect of the amount of CRL added, **b** The effect of the immobilization time of CRL. The enzyme immobilization was conducted in phosphate buffer solution (0.1 M, pH = 7.0) at 37 °C

Discussion

Figure 9 displays the reaction mechanism of polydopamine modified Fe_3O_4@GNSs in this work. The Fe_3O_4 doped graphite nanosheets were firstly prepared by a one-pot hydrothermal method, the process of which is a versatile chemical approach for the synthesis of nano-materials with well-defined shapes and controlled sizes. Compared with the similar Fe_3O_4 decorated graphene, graphene oxide and reduced graphene oxide synthesis [35–37], graphite nanosheets obtained from the expanded graphite is more economical-effective, manufacture easily and environmentally friendly. Then, the adhesive-polymer (PDA) was deposited on the surface of Fe_3O_4@GNSs uniformly via the dip-coating way (tris-buffer solution, pH 8.5). The familiar adhesion between PDA platform and Fe_3O_4@GNSs composite is fast, green and process controllable, and the versatile chemical properties as a binding regent and the excellent biocompatibility of PDA film played an important role in CRL immobilization.

In this work, the self-polymerization of DA formed a thin, surface-adherent PDA film onto Fe_3O_4@GNSs under a controllable condition. Its bioactive surface can graft macromolecules directly via Schiff base formation between animo

Table 1 Optimal conditions of immobilizing lipase

Support	Lipase amount added (mg/g)	Time (*h*)	pH	Protein bound (mg/g support)	Immobilization yield (%)	Activity recovery (%)
Fe_3O_4@GNSs-PDA	350	5	7	337.96	96.56	65.43

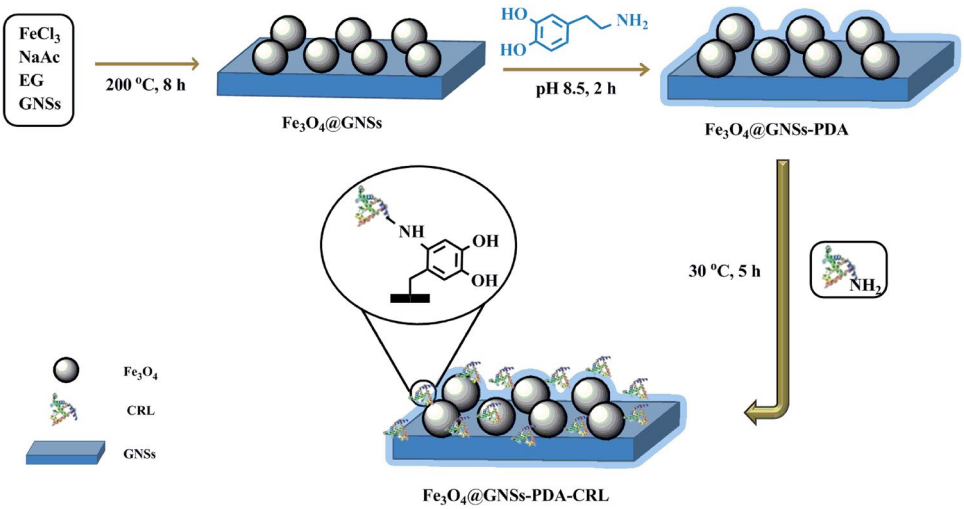

Fig. 9 Schematic illustration of the synthesis process used to produce Fe_3O_4@GNSs-PDA and CRL immobilized on Fe_3O_4@GNSs-PDA

group of macromolecules and quinone group of PDA [32] along with some physical effects by the noncovalent functionalities such as amino and hydroxyl groups as well as π–π bonds [29]. Compared with many related works which usually use some synthetic reagents (such as glutaraldehyde, epichlorohydri, formaldehyde, carbodiimide (EDC), and hexamethy-lene-1,6-diamino-carboxysulphonate (HDACS)) as the cross-linkers between supporting materials and enzymes [45, 46], we provided a fast, effective, and most importantly, non-toxic process for lipase immobilization. Additionally, the chemical stability, high affinity of GNSs also contributed to the effective lipase immobilization. Fe_3O_4 nanoparticles embedded in GNSs not only acted as an easy separation tool in Fe_3O_4@GNSs-PDA composites, but also mitigated the restacking and aggregation of GNSs during the one-pot process. The principle of CRL immobilized on Fe_3O_4@GNSs-PDA composite is illustrated in Fig. 9.

Optimal conditions of enzymatic activity

The effect of pH value on the activity of ICRL is given in Fig. S1A. The optimal pH of both free CRL and ICRL is 7.0. In addition, compared to the pH endurance of free CRL, ICRL showed enhanced stability especially in the alkaline zone. It can be explained that by covalent attachment, the configuration of lipase was fixed on the surface of Fe_3O_4@GNSs-PDA so the tolerability of CRL to pH in surroundings increased [49]. The abundant–OH/-O^- pairs and the–NH_2/-NH_3^+ pairs on PDA made it a zwitter-ion under different pH range, which could tune the local pH value. Thus the immobilized CRL would stay in the buffer region against the environmental mutation. This indicates that the lipase immobilized on Fe_3O_4@GNSs-PDA possesses markedly improved adaptability in a wide pH range, which can greatly expand the applications of lipase in chemical and biocatalytic industry.

The operating temperature range is another important factor in limiting the practical applications of lipase. Figure S1B shows the effect of temperature of the solutions on the hydrolysis activity of free and immobilized lipase for olive oil. The optimum reaction temperature of both free and immobilized lipase is 30 °C, while the activity of free lipase decreased sharply with the increase of the temperature. Compared with free lipase, the ICRL kept its relative activity up to 80 % in the temperature range of 20–60 °C and exhibited the high relative activity of 42 % at 90 °C, revealed much superb heat endurance than that of the free lipase. The increase of the optimum reaction temperature for the immobilized CRL may be due to the covalent combination between the Fe_3O_4@GNSs-PDA and lipase as well as the change of the conformational integrity in lipase structure. Moreover, the protective effect provided by the flexible structure of the prepared Fe_3O_4@GNSs-PDA also conducted a tough performance with enzymes from denaturation at high temperature.

The strong thermal stability is one of the critical factors in the industrial applications. Figure S2A shows the residual activity of free and immobilized lipase at 50 °C on the hydrolysis reaction of olive oil. Both the free CRL and ICRL exhibited the similar trend: the residual activity declined along with the reaction time prolonged. While the ICRL declined less and more slowly compared with the free form. After 150 min, free CRL lost the activity while ICRL kept it at 30 % and did not lose activity when the reaction time was at 240 min. These results probably resulted from the excellent thermal tolerance, good mechanical hardness and high specific surface area of the prepared supporting material, which protected the CRL from unfolding and prevented conformational transitions.

A denaturant such as urea can cause the protein to unfold, which may highly restrict the industrial applications of lipase. In order to investigate the influence of denaturant on the inactivation of lipase, the effect of urea with different concentrations on the hydrolysis activity of free and immobilized lipase was determined at 30 °C in phosphate buffer (0.1 M, pH = 7.0). From Fig. S2B we can see the activity of CRL shows a progressive loss with the concentration increase of urea. The CRL showed a reasonable decrease and significantly prevented from denaturation after immobilization on Fe_3O_4@GNSs-PDA composite. The ICRL kept the excellent residual activity of 87 % in 3 M urea and still held it at about 75 % in 6 M urea. However, free lipase possessed only 21 % activity in 3 M urea and deactivated totally when the concentration of urea was up to 6 M, respectively. One of the possible reasons is the lipase was attached on Fe_3O_4@GNSs-PDA mainly via covalent bonding, and it is possibly conducted a higher activation energy for the molecules to recognize and prevented the ternary structure of lipase from denaturation [50].

In order to achieve the reuse of lipase and then for the potential application in industry, it is important to investigate the well reusability of lipase. The variation of the activity of the ICRL after multiple-reuse was shown in Fig. 10. It can be observed from Fig. 10 that the ICRL kept the high activity at 80 % after 12 recycles. The decline in activity was considered as the denaturation and leakage of protein after some reaction circles. Thus, it can be concluded that the Fe_3O_4@GNSs-PDA could significantly increase the operational stability as well as confer additional stability against denaturation and provide a protected microenvironment that could enhance the catalytic properties of the biocatalyst.

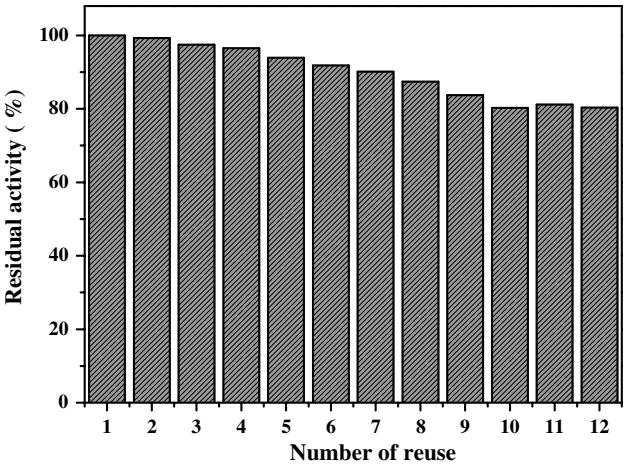

Fig. 10 Number of reuses of the immobilized CRL. The recovered CRL was washed with phosphate buffer solution (0.1 M, pH = 7.0) thoroughly and reused for the next cycle. The enzyme activity was compared with the first running (activity defined as 100 %)

Conclusion

In this work, mussel-inspired magnetic graphite composite was successfully synthesized via the simple dip-coating way of dopamine. Then the as-prepared composite was used to immobilize CRL covalently under mild conditions and avoided any other toxic functional chemicals. The novel Fe_3O_4@GNSs-PDA composite was proved to possess high magnetization, a uniform well-defined structure and high affinity towards lipase immobilization. By means of measuring various properties of ICRL, the Fe_3O_4@GNSs-PDA composite was demonstrated to have high capacity and well biocompatibility for lipase immobilization, and the Fe_3O_4@GNSs-PDA immobilized CRL showed excellent abilities in environmental stability and catalytic activities. Significantly, the ICRL retained 80 % activity after 12 times of recycling for batch hydrolysis of olive oil emulsion. Overall, the successful application in enzyme immobilization using the adhesive magnetic graphite composite confirmed the suitability for various biochemical applications.

Acknowledgments The authors thank the financial supports from the National Natural Science Foundation of China (No. 21374045), the scientific research ability training of under-graduate students majoring in chemistry by the two patters based on the tutorial system and top students (J1103307) and the Opening Foundation of State Key Laboratory of Applied Organic Chemistry (SKLAOC-2009-35).

Conflict of interest The authors declare no competing financial interest.

References

1. Garcia J, Zhang Y, Taylor H, Cespedes O, Webb ME, Zhou DJ (2011) Multilayer enzyme-coupled magnetic nanoparticles as efficient, reusable biocatalysts and biosensors. Nanoscale 3:3721–3730
2. Ince A, Bayramoglu G, Karagoz B, Altintas B, Bicak N, Arica MY (2012) A method for fabrication of polyaniline coated polymer microspheres and its application for cellulase immobilization. Chem Eng J 189–190:404–412
3. Torres CF, Hill CG Jr (2004) Lipase-catalyzed acidolysis of butter oil with conjugated linoleic acid: a kinetic study involving multiple reuse of the immobilized enzyme. Ind Eng Chem Res 43:3714–3722
4. Sanchez S, Demain AL (2011) Enzymes and bioconversions of industrial, pharmaceutical, and biotechnological significance. Org Process Res Dev 15:224–230
5. Kim JB, Grate JW, Wang P (2006) Nanostructures for enzyme stabilization. Chem Eng Sci 61:1017–1026
6. Chang SW, Shaw JF, Yang KH, Chang SF, Shieh CJ (2008) Studies of optimum conditions for covalent immobilization of < i > Candida rugosa </i > lipase on poly (γ-glutamic acid) by RSM. Bioresour Technol 99:2800–2805
7. Grunwald P, Hansen K, Gunßer W (1997) The determination of effective diffusion coefficients in a polysaccharide matrix used for the immobilization of biocatalysts. Solid State Ionics 101–103:863–867
8. Shen WZ, Ren LW, Zhou H, Zhang SC, Fan WB (2011) Facile one-pot synthesis of bimodal mesoporous carbon nitride and its function as a lipase immobilization support. J Mater Chem 21:3890–3894
9. Yang XW, Cai ZW, Ye ZM, Chen S, Yang Y, Wang HF (2012) In situ synthesis of porous silica nanoparticles for covalent immobilization of enzymes. Nanoscale 4:414–416
10. Mei L, Xie R, Yang C, Ju XJ, Wang W, Wang JY (2013) pH-responsive Ca-alginate-based capsule membranes with grafted poly(methacrylic acid) brushes for controllable enzyme reaction. Chem Eng J 232:573–581
11. Xu R, Zhou QJ, Li FT, Zhang BR (2013) Laccase immobilization on chitosan/poly(vinyl alcohol) composite nanofibrous membranes for 2,4-dichlorophenol removal. Chem Eng J 222:321–329
12. Geim AK (2009) Graphene: status and Prospects. Science 324:1530–1534
13. Bak JM, Lee H (2012) pH-tunable aqueous dispersion of graphene composites functionalized with poly (acrylic acid) brushes. Polymer 53:4955–4960
14. Eswaraiah V, Balasubramaniam K, Ramaprabhu S (2012) One-pot synthesis of conducting grapheme-polymer composites and their strain sensing application. Nanoscale 4:1258–1262
15. Liang RP, Liu CM, Meng XY, Wang JW, Qiu JD (2012) A novel open-tubular capillary electrochromatography using β-cyclodextrin functionalized graphene oxide-magnetic composite s as tunable stationary phase. J Chromatogr A 1266(95–102):17
16. Lin Y, Tao Y, Pu F, Ren J, Qu X (2011) Combination of graphene oxide and thiol-activated DNA metallization for sensitive fluorescence turn-on detection of cysteine and their use for logic gate operations. Adv Funct Mater 21:4565–4572
17. Feng L, Wu L, Wang J, Ren J, Miyoshi D, Sugimoto N (2012) Detection of a prognostic indicator in early-stage cancer using functionalized graphene-based peptide sensors. Adv Mater 24:125–131
18. Nam B, Lee HJ, Goh H, Lee YB, Choi WS (2012) Sandwich-like graphene composite s armed with nanoneedles. J Mater Chem 22:3148–3153
19. Zhang Y, Zhang J, Huang X, Zhou X, Wu H, Guo S (2012) Assembly of graphene oxide-enzyme conjugates through hydrophobic interaction. Small 8:154–159
20. Chen L, Wei B, Zhang XT, Li C (2013) Bifunctional graphene/γ-Fe2O3 hybrid aerogels with double nanocrystalline networks for enzyme immobilization. Small 9:2331–2340
21. Ma YX, Li YF, Zhao GH, Yang LQ, Wang JZ, Shan X (2011) Preparation and characterization of graphite nanosheets decorated with Fe3O4 nanoparticles used in the immobilization of glucoamylase. Carbon 50:2976–2986
22. Cheng G, Liu YL, Wang ZG, Zhang JL, Sun DH, Ni JZ (2012) The GO/rGO-Fe3O4 composites with good water-dispersibility and fast magnetic response for effective immobilization and enrichment of biomolecules. J Mater Chem 22:21998–22004
23. Li XH, Zhu H, Feng J, Zhang JW, Deng X, Zhou BF (2013) One-pot polylol synthesis of graphene decorated with size- and density-tunable Fe3O4 nanoparticles for porcine pancreatic lipase immobilization. Carbon 60:488–497
24. Kang K, Choi IS, Nam Y (2011) A biofunctionalization scheme for neural interfaces using polydopamine polymer. Biomaterials 32:6374–6380
25. Lee H, Dellatore SM, Miller WM, Messersmith PB (2007) Mussel-inspired surface chemistry for multifunctional coatings. Nature 318:426–430
26. Chen X, Yan Y, Mullner M, Koeverden MP, Noi KF, Zhu W (2014) Engineering fluorescent poly(dopamine) capsules. Langmuir 30:2921–2925
27. Yan YH, Zheng ZF, Deng CH, Zhang XM, Yang PY (2013) Facile synthesis of Ti4 + -immobilized Fe3O4@ polydopamine core–shell microspheres for highly selective enrichment of phosphopeptides. Chem Commun 49:5055–5057
28. Hoa CC, Ding SJ (2014) Dopamine-induced silica–polydopamine hybrids with controllable morphology. Chem Commun 50:3602–3605
29. Faure E, Daudré CF, Jérôme C, Lyskawa J, Fournier D, Woisel P (2013) Catechols as versatile platforms in polymer chemistry. Prog Polym Sci 38:236–270
30. Ma ZY, Jia X, Hu JM, Zhang GX, Zhou F, Liu ZY (2013) Dual-responsive capsules with tunable low critical solution temperatures and their loading and release behavior. Langmuir 29:5631–5637
31. Raghavendra T, Basak A, Manocha LM, Shah AR, Madamwar D (2013) Robust nanobioconjugates of Candida antarctica lipase B-Multiwalled carbon nanotubes: characterization and application for multiple usages in non-aqueous biocatalysis. Bioresource Technol 140:103–110
32. Martín M, Salazar P, Villalonga E, Campuzano S, Pingarrónd JM, González-Mora JL (2014) Preparation of core-shell Fe3O4@ poly(dopamine) magnetic nanoparticles for biosensor construction. J Mater Chem B 2:739–746
33. Bradford MM (1976) A rapid and sensitive method for the quantitation of microgram quantities of protein utilizing the principle of protein-dye binding. Anal Biochem 72:248–254
34. Ren LL, Huang S, Fan W, Liu TX (2011) One-step preparation of hierarchical superparamagnetic iron oxide/grapheme composites via hydrothermal method. Appl Surf Sci 258:1132–1138
35. Kassaee MZ, Masrouri H, Movahedi F (2011) Sulfamic acid-functionalized magnetic Fe3O4 nanoparticles as an efficient and reusable catalyst for one-pot synthesis of a-amino nitriles in water. Appl Catal A Gen 395:28–33
36. Watanabe N, Yasude O, Yasuji M, Koichi Y (1977) Isolation and identification of alkaline lipase producing microorganisms, cultural conditions and some properties of crude enzyme. Agric Biol Chem 41:1353–1358

37. Zhao S, Asuha S (2010) One-pot synthesis of magnetite nanopowder and their magnetic properties. Powder Technol 197:295–297
38. Deng H, Li XL, Peng Q, Wang X, Chen JP, Li YD (2005) Monodisperse magnetic single-crystal ferrite microspheres. Angew Chem Int Edit 44:2782–2785
39. Song C, Wu D, Zhang F, Liu P, Lu Q, Feng X (2012) Gemini surfactant assisted synthesis of two-dimensional metal nanoparticles/graphene composites. Chem Commun 48:2119–21121
40. Wang YX, Wang SH, Niu HY, Ma YR, Zeng T, Cai YQ, Meng ZF (2013) Preparation of polydopamine coated Fe3O4 nanoparticles and their application for enrichment of polycyclic aromatic hydrocarbons from environmental water samples. J Chromatogr A 1283:20–26
41. Ferrari AC, Robertson J (2000) Interpretation of Raman spectra of disordered and amorphous carbon. Phys Rev B 61:14095–14107
42. Liu YQ, Gao L, Sun J, Wang Y, Zhang J (2009) Stable Nafion-functionalized graphene dispersions for transparent conducting films. Nanotechnology 20:465605–465611
43. Alwarappan S, Erdem A, Liu C, Li CZ (2009) Probing the electrochemical properties of graphene nanosheets for biosensing applications. J Phys Chem C 113:8853–8857
44. Fei B, Qiana BT, Yanga ZY, Wanga RH, Liu WC, Mak CL (2008) Coating carbon nanotubes by spontaneous oxidative polymerization of dopamine. Carbon 46:1792–1828
45. Nagai N, Kumasaka N, Kawashima T, Ka JH, Nishizawa M, Abe T (2010) Preparation and characterization of collagen microspheres for sustained release of VEGF. J Mater Sci-Mater M 21:1891–1898
46. Powell HM, Drexler JW (2011) Dehydrothermal crosslinking of electrospun collagen. Tissue Engineering Part C-Meth 17:9–17
47. Liu X, Chen X, Li YF, Wang XY, Peng XM, Zhu WW (2012) Preparation of superparamagnetic Fe3O4@Alginate/Chitosan nanospheres for candida rugosa lipase immobilization and utilization of layer-by-layer assembly to enhance the stability of immobilized lipase. Appl Mater Interfaces 4:5169–5178
48. Liu T, Zhao YD, Wang XF, Li X, Yan YJ (2013) A novel oriented immobilized lipase on magnetic nanoparticles in reverse micelles system and its application in the enrichment of polyunsaturated fatty acids. Bioresource Technol 132:99–102
49. Mateo C, Palomo JM, Fernandez LG, Guisan JM, Fernandez LR (2007) Improvement of enzyme activity, stability and selectivity via immobilization techniques. Enzyme Microb Technol 40:1451–1463
50. Rabbani G, Ahmad E, Zaidi N, Fatima S, Khan RH (2012) pH-induced molten globule state of Rhizopus niveus lipase is more resistant against thermal and chemical denaturation than its native state. Cell Biochem Biophys 62:487–499